Chapter 5. Slot Antennas for Hyperthermia Applications at 2.45 GHz ISM Band

This chapter is based on the designing of slot antennas for hyperthermia applications at 2.45 GHz which is divided into two parts. The first part a cross-slot patch antenna and in second part designed a corner-slot patch antenna are presented.

5.1. Cross Slot Antenna for Hyperthermia Applications at 2.45 GHz

5.1.1. Introduction

This research focuses on the creation and advancement of an innovative cross-slot antenna that operates at 2.45 GHz within the ISM band. The antenna's design, simulation, fabrication, measurement, and evaluation were conducted to investigate its Specific Absorption Rate (SAR) for hyperthermia applications. Notably, this proposed antenna stands out for its capability to operate at the upper Industrial, Scientific, and Medical band of 2.45 GHz, achieving a similar SAR level to that of TEL phantom tissue, thereby addressing an important research gap.

5.1.2. Antenna Design

The process of designing and analyzing antennas involved utilizing the ANSYS HFSS v 2020R1 simulator tool. For the analysis, a human phantom model with multiple layers was created and positioned close to the antenna, with a separation distance of 2 mm. Fig. 5.1(a) to 5.1(d) refers to the evaluation steps of the proposed structure. Equations (5.1-5.4) are used for developing a simple square patch antenna to begin the design process [119]. The antenna adjustments are carried out using slots varying in size. It is evident that the antenna performance has increased from antenna-1 to antenna-4 in terms of $|S_{11}|$, and that this improvement in current distribution has allowed the antenna to operate at the desired frequency. Antenna-1 resonance occurs at 1.72 GHz with $|S_{11}|$ of -14.97 dB, where current flow is only concentrated on the edges of the patch. A cross is cut from the top of the patch as shown in Fig. 5.1(b) and observed that $|S_{11}|$ shifts to lower bands with poor isolation as shown in Fig.4. Equations (5.5) and (5.6) are used to determine the slots' dimensions [125, 126]. As illustrated in Fig. 5.1(c), unite this slot with L-slots in all four locations to produce good isolation at lower bands. Adding slots increases the overall electrical length of the surface current, resulting in a frequency shift from the higher band to the lower band. The last step involves chamfering a square section measuring 10×10 mm^2 from the patch's edges so that the original dimension of the patch gets reduced therefore resonating frequency is shifting towards higher band i.e.at 2.45 GHz. The multiple slots in a collinear fashion will increase the superposition of the electric field which is a viable solution for increasing the temperature near the cancerous tissue, which intends to increase the SAR value.

The length of the patch is given as [119],

$$L = \frac{1}{2f_r\sqrt{\varepsilon_{reff}}\sqrt{\mu_0\varepsilon_0}} - 2\Delta L \tag{5.1}$$

Where,

$$\frac{\Delta L}{h} = 0.412\frac{(\varepsilon_{reff}+0.3)(\frac{W}{h}+0.264)}{(\varepsilon_{reff}-0.258)(\frac{W}{h}+0.8)} \tag{5.2}$$

Where, h is the thickness of the substrate and W is the width of the patch, and ε_{reff} is the effective dielectric constant of the proposed antenna,

$$\varepsilon_{reff} = \frac{\varepsilon_r+1}{2} + \frac{\varepsilon_r-1}{2}\left[1+12\frac{h}{W}\right]^{-1/2} \tag{5.3}$$

$$W = \frac{v_0}{2f_r}\sqrt{\frac{2}{\varepsilon_r+1}} \tag{5.4}$$

Where, v_0 is the free-space velocity of light.

The length of the slot is given as [125],

$$L_{slot} = \frac{\lambda_g}{4} = \frac{c}{4f\sqrt{\frac{\epsilon_r+1}{2}}} \tag{5.5}$$

The width of the slot is given as [126],

$$w_{slot} = \frac{\lambda}{60} \tag{5.6}$$

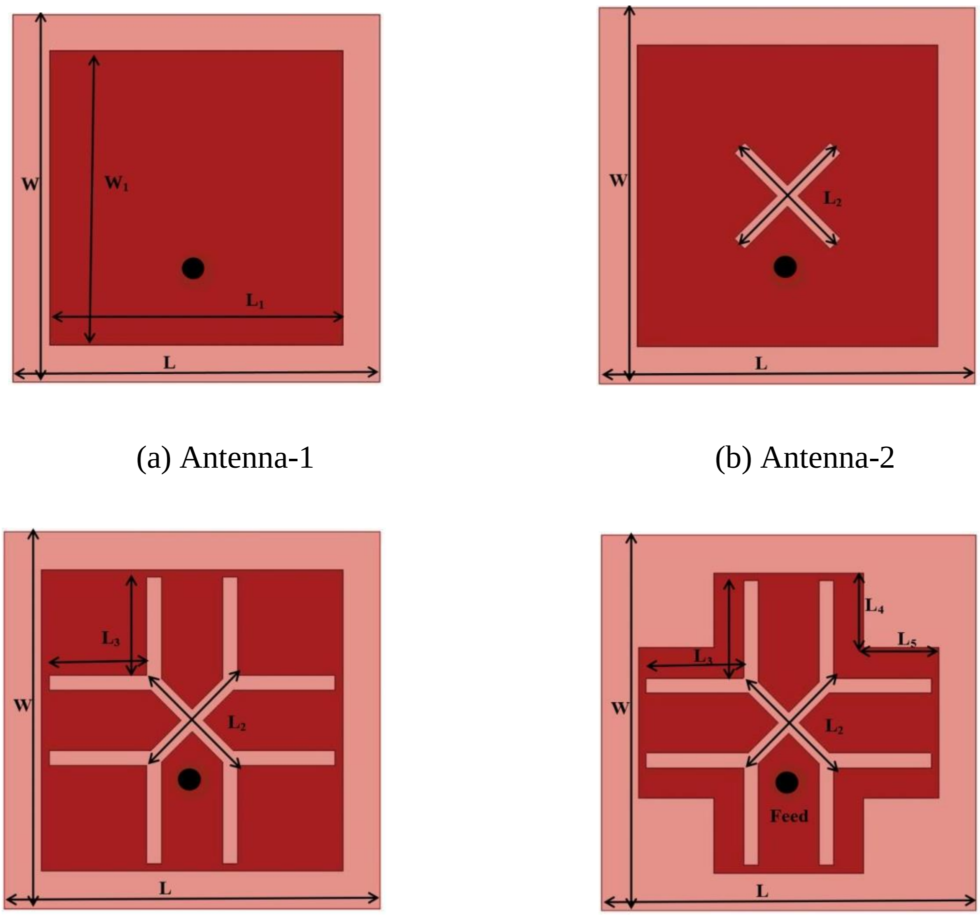

(a) Antenna-1

(b) Antenna-2

(c) Antenna-3

(d) Proposed antenna

Figure 5.1 The geometrical layout of the proposed antenna.

Table 5.1 Geometric characteristics of the proposed antenna

Parameter	Value (mm)	Parameter	Value (mm)
L	50	L_3	13
W	50	L_4	10
L_1	40	L_5	10
W_1	40	R_{in}	0.47
L_2	9.5	W	2

5.1.3. Phantom Model

ANSYS HFSS v 2020R1 simulator tool was utilized for simulation purposes. To mimic the human environment, a single-layered TEL phantom was constructed. The dimensions of the phantom measured 90×90×26.27 (mm^3) [127]. The composition of the TEL phantom's materials, expressed as a percentage by weight, includes DGBE (Diethylene glycol butyl ether), NaCl, Triton X-100, and water, with respective proportions of 7.99, 0.16, 19.97, and 71.88 [128-130]. The electrical characteristics of the TEL were set to be frequency-dependent, with permittivity decreasing and conductivities increasing with frequency [122, 131]. The measured dielectric properties of the TEL phantom at 2.45 GHz were as follows: permittivity (ϵ_r) of 60.36, conductivity (σ) of 1.83437 S/m, and density (ρ) of 1100 kg/m^3. The antenna, situated at a height of 2 mm, was integrated with the TEL, and its upper surface faced the water bolus surface.

5.1.4. Results and Discussion

5.1.4.1. Reflection Coefficient

The performance of the cross-slot antenna was thoroughly evaluated through both simulation and measurement using TEL phantom tissue. The results depicted in Fig. 5.2 indicate the reflection coefficient values at each step, with the proposed antenna achieving a remarkable -20.08 dB. Furthermore, Fig. 5.3 illustrates a comparison between the simulated and measured reflection coefficient outcomes when the antenna is tested with TEL phantom tissue, showing values of -15.91 dB and -16.92 dB, respectively. The tissue loading, however, causes a slight frequency of detuning [132].

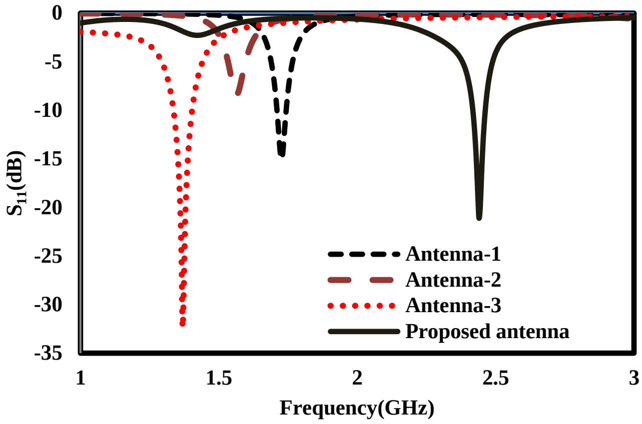

Figure 5.2 Simulated reflection coefficient results of all steps

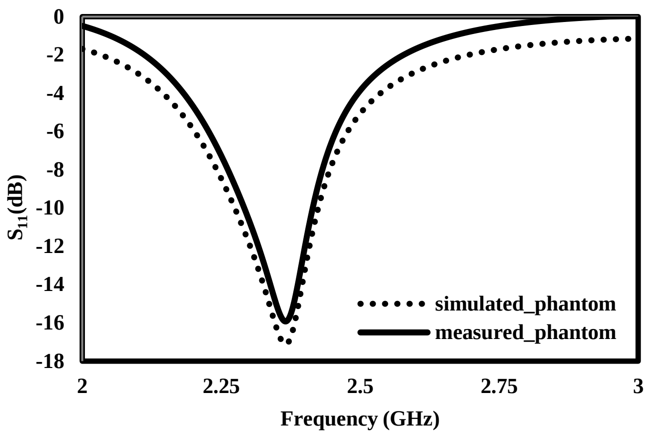

Figure 5.3 Reflection coefficient results with phantom

5.1.4.2. SAR and Radiation Pattern

According to the IEEE C95.1-1999 standard, the Specific Absorption Rate (SAR) should conform to a maximum peak average SAR value of 1.6 W/kg for 1 gram of tissue [29]. Analyzing the numerical study of SAR with the TEL phantom model at 2.45 GHz was done using HFSS software. The transmitted power to the proposed antenna is 1 W, Fig.5.4 depicts the SAR distribution. The proposed antenna has multiple slots in a collinear fashion which will increase the superposition of the electric field which is a viable solution for increasing the temperature. From equation (5.7) SAR is directly proportional to the square of the electric field, which indicates the SAR value will increase with increasing E-field. The maximum SAR value is 404.15 W/kg with a maximum acceptable input power of 3.9 mW. Analysis of the SAR value of the proposed antenna encounters the IEEE evaluation standard.

$$SAR = \frac{\sigma E^2}{2\rho} \quad \text{W/kg} \tag{5.7}$$

Simulated and measured radiation patterns in the XZ and YZ plane for the E-plane and H-plane at 2.45 GHz are shown in Fig.5.5. The peak simulated and measured gain attained at 2.45 in the case of the E-plane is -5.1 dBi and -8.6 dBi, respectively, and for the case of the H-plane, it is -5.4 dBi and -7.4 dBi respectively. By analyzing Fig. 5.5, it becomes evident that the radiation patterns exhibit omnidirectional characteristics due to the symmetrical structure in both the XZ and YZ planes. This desirable feature makes the antenna suitable for various biomedical applications.

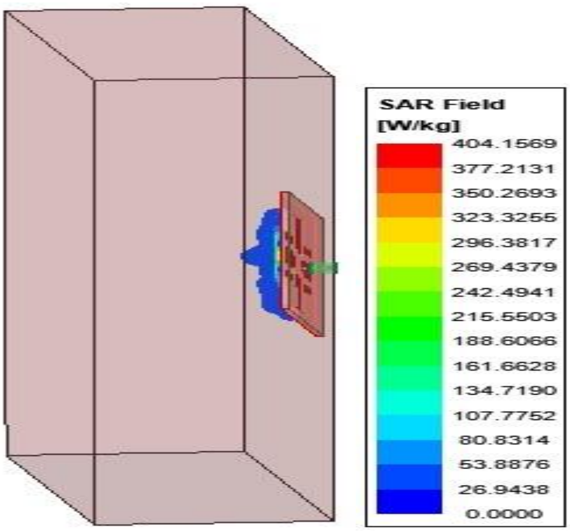

Figure 5.4 SAR contour plot

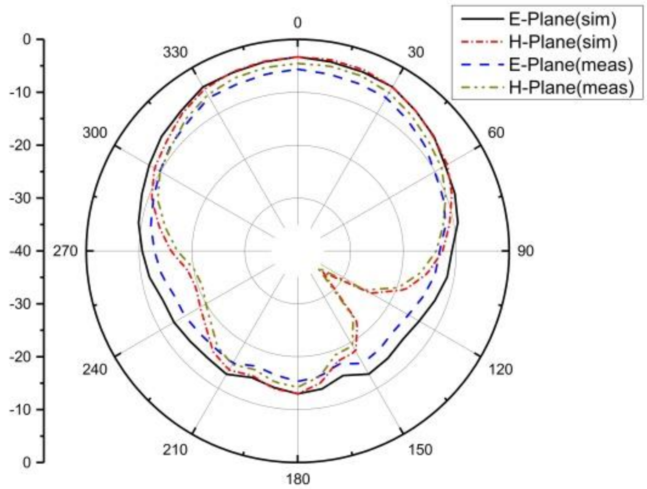

Figure 5.5 Radiation pattern plot

5.1.4.3. Fabrication and Measurement

The proposed antenna's prototype, fabricated on an FR-4 substrate with a relative permittivity of 4.4 and a thickness of 1.6 mm, is shown in Fig. 5.6(a). The reflection coefficient was determined using an R&S(ZNB8) vector network analyzer with a frequency range of (9kHz-8.5GHz), as shown in Fig. 5.6(b). For the calculation of SAR first of all, measured the electric field intensity inside the TEL phantom as shown in Fig.5.6(c). In this setup, a signal generator R&S SMR 40(100 MHz-40 GHz) was used as a source, and a spectrum analyzer R&S FSH8(100 kHz-8 GHz) was used for reading the electric field intensity value. Finally, the measured SAR value was calculated using equation (5.7).

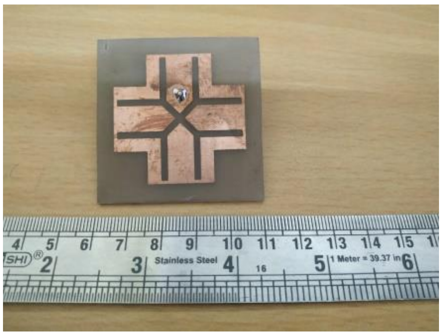

(a)

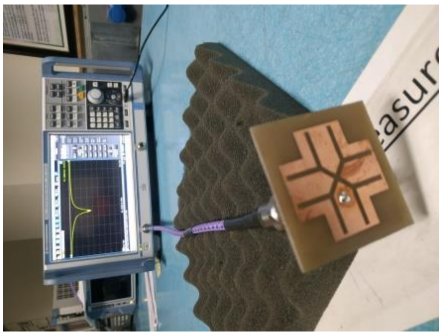

(b)

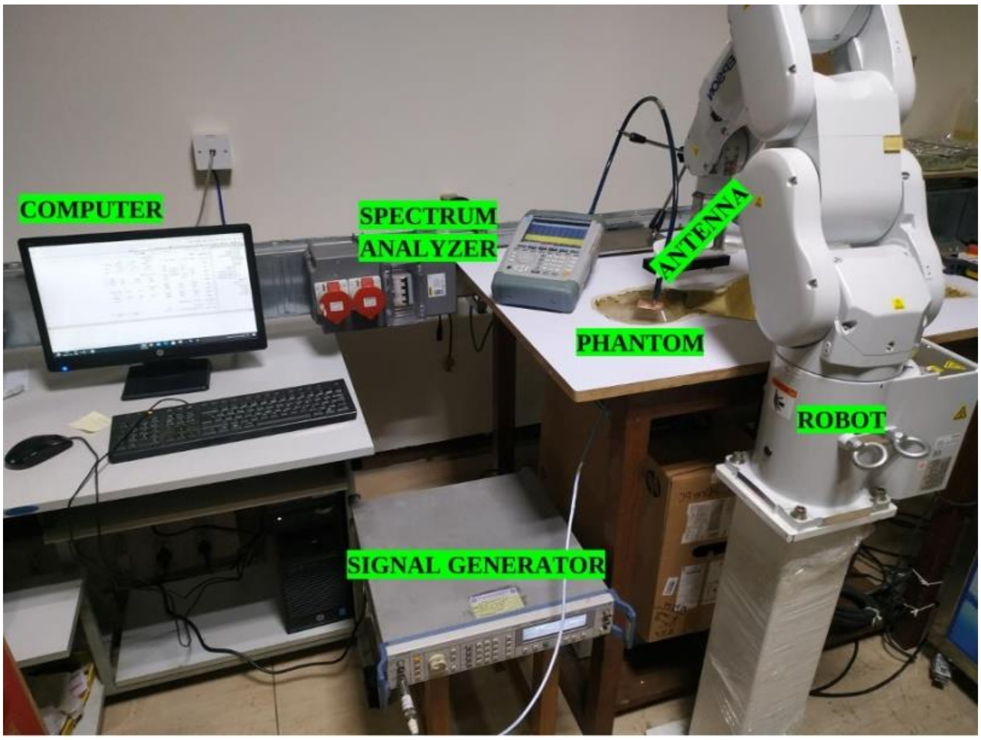

(c)

Figure 5.6 (a) Fabrication prototype (b) S_{11} measurement (c) SAR measurement setup

Table 5.2 Compares reported antennas to proposed antenna qualitatively

Ref.	Freq. (GHz)	Size (mm^3)	S_{11} (dB)	SAR (W/kg)	Gain (dBi)	App.
[133]	2.48	24×22×0.07	-34.68	0.914	-19.7	ISM
[127]	2.45	10×10×1.27	-25	254.74	-22.33	ISM
[129]	2.45	22.5×22.5×2.5	-26	NA	-11	ISM
[130]	2.45	19.8×19.4×1.27	-25	314	-22	ISM
[131]	2.4	50×50×4	-21.6	NA	-27	ISM
[132]	2.45	$\pi \times 25^2 \times 5$	-25	7.47	-5.1	ISM
Work	**2.45**	**50×50×1.6**	**-20.08**	**404.15**	**-5.1**	**ISM**

The resonance of the proposed antenna at a higher ISM band demonstrates superior SAR value, adhering to IEEE standards. Additionally, when compared to the antenna design presented in the aforementioned literature, our antenna showcases improved performance in various parameters, as evident from Table 5.2.

5.1.5. Summary

This research presents a novel cross-slot antenna for a 2.45 GHz hyperthermia application. Results for the suggested antenna's reflection coefficient, surface current density plot, SAR, and radiation plot are obtained. The antenna performance is superior to that of previous research papers that have been released. SAR value is within the range allowed for exposed bodies according to IEEE guidelines. The antenna was constructed with measurement in mind. The simulation results' reliability and validity are confirmed. According to the aforementioned specifications, the suggested antenna can be used in applications involving hyperthermia.

Further, reduce the size of the ISM band antenna by modifying the new novel corner-slot antenna in the upcoming section 5.2 of this chapter.

5.2. Corner Slot Antenna for Hyperthermia Applications at 2.45 GHz

5.2.1. Introduction

In this part, we present the design, simulation, and experimental results of a microstrip slot antenna for hyperthermia application at 2.45 GHz. The proposed antenna is designed to operate in the ISM band, which is widely used for various medical applications. The antenna's slot configuration and the substrate's dielectric constant are optimized to achieve a resonant frequency of 2.45 GHz and high radiation efficiency.

The rest of the chpter is organized as follows: Section II provides a detailed description of the antenna design and simulation methodology as well as phantom tissue model making and its dielectric properties measurements. Section III presents the experimental results, including the antenna's return loss, radiation pattern, and specific absorption rate (SAR) values. Finally, the chapter concludes with a discussion of the results and the potential applications of the proposed antenna in hyperthermia treatment.

5.2.2. Antenna Design

FEM is a powerful tool to study the proposed antenna performance. The electromagnetic wave propagating in coaxial feed can be described by transverse electromagnetic fields (TEM). By considering time-harmonic fields, wave propagation can be described by equations (5.8)-(5.10) [134].

$$E = e_r \frac{C}{r} e^{j(\omega t - kz)} \tag{5.8}$$

$$H = e_{r\varphi} \frac{C}{R} e^{j(\omega t - kz)} \tag{5.9}$$

$$P_{avg} = e_z \frac{C^2}{Z} ln\left(\frac{r_{inner}}{r_{outer}}\right) \tag{5.10}$$

Where,

$$k = \frac{2\pi}{\lambda} \qquad (5.11)$$

Where r, φ, and z are the cylindrical coordinates of the coaxial cable, z is the direction of propagation, Z is the wave impedance in the cable dielectric, P_{avg} is the average power flow, r_{inner} and r_{outer} correspond to the radius of the inner and outer conductor.

And Maxwell's equations that govern the antenna behaviour are shown in (5.12)-(5.15) [135],

$$\varDelta \times E = -j\omega\overleftrightarrow{\mu}.H - M_{imp} \qquad (5.12)$$

$$k = \frac{2\pi}{\lambda}\varDelta \times H = -j\omega\overleftrightarrow{\epsilon}.E - J_{imp} \qquad (5.13)$$

$$\varDelta.(\overleftrightarrow{\epsilon}.E) = -\frac{1}{j\omega}\nabla.J_{imp} \qquad (5.14)$$

$$k = \frac{2\pi}{\lambda}\varDelta.(\overleftrightarrow{\mu}.H) = -\frac{1}{j\omega}\nabla.M_{imp} \qquad (5.15)$$

Where M_{imp} is the magnetic current density, J_{imp} is the current source that excited the antenna.

To correctly determine the antenna performance, it is important to define the boundary conditions. Because the antenna irradiates an EM field to infinity, the solution space must be limited to a finite space (S_0) [135].

$$k = \frac{2\pi}{\lambda}\hat{n}\times \nabla \times \binom{E}{H} + jk_0\hat{n} \times \hat{n} \times \binom{E}{H} \approx 0 \qquad r \in S_0 \qquad (5.16)$$

The finite space S_0 must be set at least a half-wavelength away from the antenna.

$$k = \frac{2\pi}{\lambda}n \times E = 0 \qquad r \in S_{PEC} \qquad (5.17)$$

Where S_{PEC} is the perfectly electrically conducting (PEC) surface of the antenna body, the antenna feed is defined as a port boundary condition of first order low reflecting boundary condition [134, 136].

$$n \times \sqrt{\epsilon E} - \sqrt{\mu H_{\varphi}} = -\sqrt{\mu H_{\varphi 0}} \quad (5.18)$$

Where,

$$H_{\varphi 0} = \frac{\sqrt{\frac{P_{avg} Z}{\pi r ln\left(\frac{r_{inner}}{r_{outer}}\right)}}}{r} \quad (5.19)$$

The length of the patch is given as [119],

$$L = \frac{1}{2 f_r \sqrt{\varepsilon_{reff}} \sqrt{\mu_0 \varepsilon_0}} - 2\Delta L \quad (5.20)$$

Where,

$$\frac{\Delta L}{h} = 0.412 \frac{(\varepsilon_{reff} + 0.3)(\frac{W}{h} + 0.264)}{(\varepsilon_{reff} - 0.258)(\frac{W}{h} + 0.8)} \quad (5.21)$$

Where, h is the thickness of the substrate and W is the width of the patch, and ε_{reff} is the effective dielectric constant of the proposed antenna,

$$\varepsilon_{reff} = \frac{\varepsilon_r + 1}{2} + \frac{\varepsilon_r - 1}{2}\left[1 + 12\frac{h}{W}\right]^{-1/2} \quad (5.22)$$

$$W = \frac{v_0}{2 f_r}\sqrt{\frac{2}{\varepsilon_r + 1}} \quad (5.23)$$

Where, v_0 is the free-space velocity of light,

The length of the slot is given as [125],

$$L_{slot} = \frac{\lambda_g}{4} = \frac{c}{4f\sqrt{\frac{\epsilon_r + 1}{2}}} \quad (5.24)$$

The width of the slot is given as [126],

$$w_{slot} = \frac{\lambda}{60} \quad (5.25)$$

Fig.5.7 shows the evaluation process of the proposed antenna, to minimize the size of the proposed antenna slots are cut in the patch. Here genetic algorithm Optimization procedures are applied to a T-slot antenna to determine the best choice of slots to search for surface current (Js) that could improve and give the best reflection coefficient at the 2.45 GHz ISM band [137]. Initially, antenna-1 was taken into consideration which is a simple patch without any slot having poor isolation Fig.5.11. After that four rectangular slots are cut at each corner which have poor isolation then after making these slots like T-slot having better isolation, because the addition of slots will increase the overall electrical length of the surface current, resulting in a frequency shift to the lower band as shown in Fig.5.11. A 50-ohm coaxial cable is used to excite the antenna [138]. The proposed antenna has been simulated using Ansys HFSS ver. 2020R1, and optimized dimensions are listed in Table 5.3.

Table 5.3 Geometrical parameters of the proposed antenna

Parameter	Value (mm)	Parameter	Value (mm)
L	26	L_3	12.72
W	26	w_1	0.707
L_1	7.72	w_2	1
L_2	11.31	R_{in}	0.47

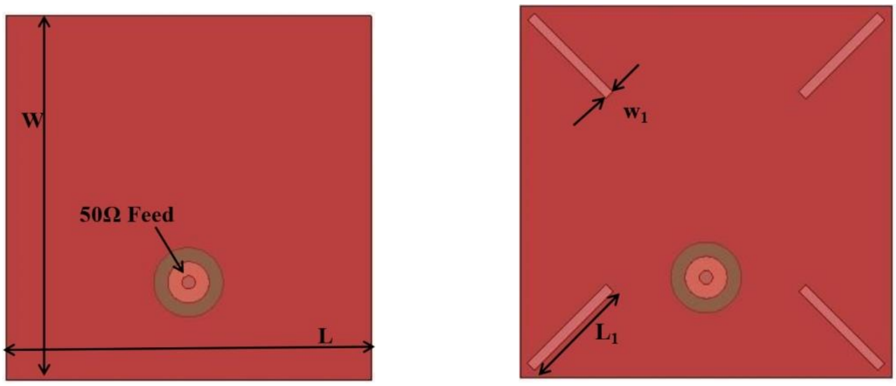

(a) Antenna-1 (b) Antenna-2

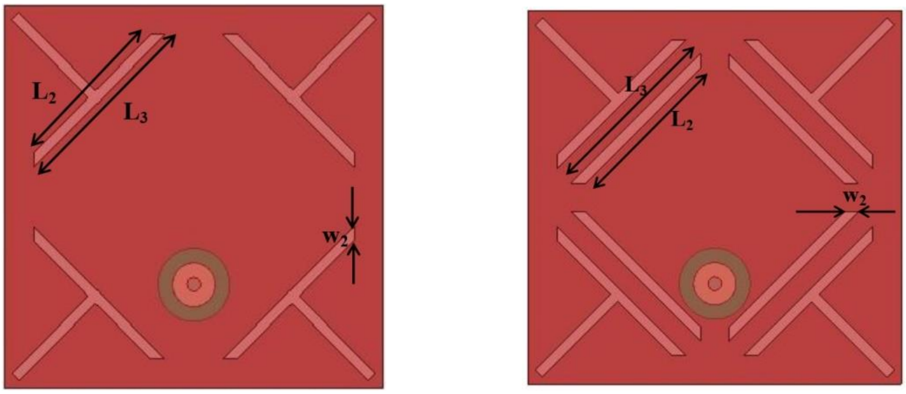

(c) Antenna-3 (d) Proposed antenna

Figure 5.7 The geometrical configuration of the proposed antenna.

5.2.3. Phantom Model

As shown in Figure 5.8, a single-layered TEL phantom is built to imitate the human environment during simulation. The dimension of the phantom is 90×90×26.27 (mm^3) [127]. The combination of material for TEL phantom percentage by weight is DGBE (Diethylene glycol butyl ether), NaCl, Triton X-100, and water are 7.99, 0.16, 19.97, and 71.88 respectively [129, 130, 139, 140]. The dielectric properties of the TEL are set frequency dependent, having permittivity that decreases and conductivities that increase with frequency [122, 131]. As shown in Fig.5.10, the TEL phantom's measured dielectric properties are permittivity (ϵ_r) of 60.36, conductivity (σ) of 1.83437 S/m and density (ρ) of 1100 kg/m^3 at 2.45 GHz. The antenna's upper surface faces the water bolus surface and is integrated with the TEL at a height of 2 mm.

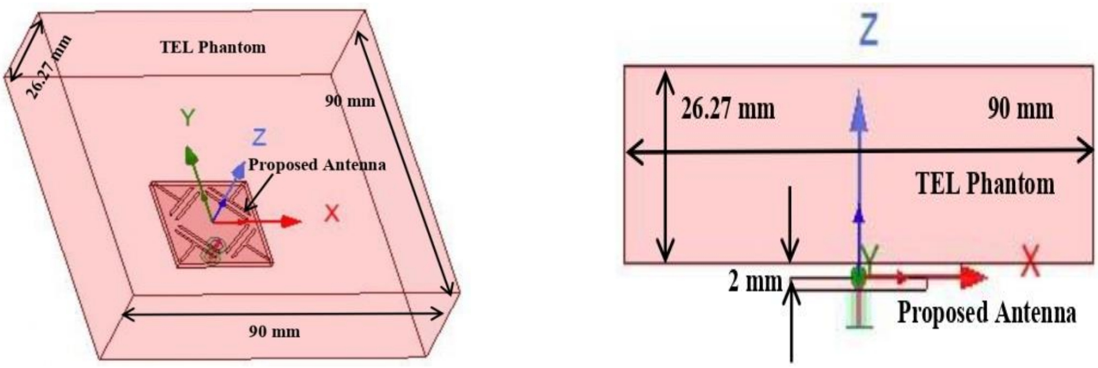

(a) 3D view (b) Side view

Figure 5.8 TEL phantom mounted with the proposed antenna.

5.2.4. Dielectric Measurement

Fig.5.9 and Fig.5.10 show the dielectric measurement setup and the measured dielectric properties graph respectively. The open-ended dielectric measurement method is used as shown in Fig.5.9, one side of the open-ended cable is connected with the R&S(ZNB8) vector network analyzer (VNA), and the other side emerges into the TEL phantom. A computer is connected to the VNA to collect the data associated with this measurement.

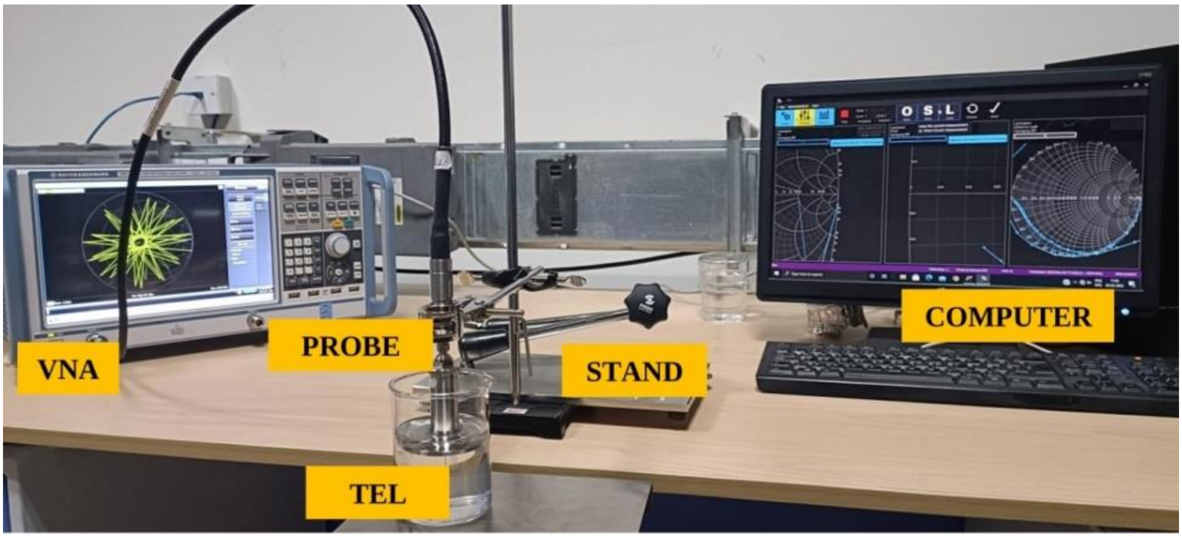

Figure 5.9 Measurement setup for dielectric properties.

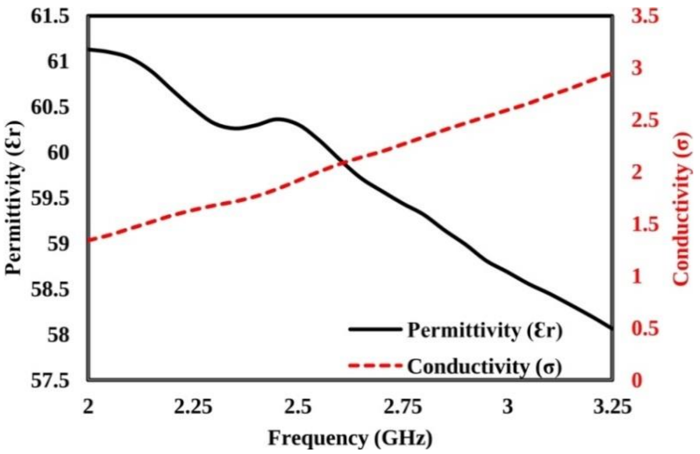

Figure 5.10 Permittivity and conductivity plots for TEL phantom.

5.2.5. Results and Discussion

5.2.5.1. Reflection Coefficient

From Fig. 5.11, it is observed that the resonant frequencies are shifting downward from 2.8, 2.7, 2.56, and 2.45 GHz, which indicates that 14.28% miniaturization is achieved in the proposed antenna with unchanged original square patch antenna-1 dimensions and substrate properties. When adding T-slot at the corners of the patch the resonant frequency shifts down. Furthermore, the rectangular slots parallel with T-slots at every corner have a great influence on the frequency of the proposed antenna. The antenna has been simulated and measured in the air as well as the TEL phantom, Fig.5.12 and Fig. 5.13 show the simulated and measured reflection coefficient results of the proposed antenna respectively. The simulated and measured reflection coefficients with air and with TEL are -17.46 dB, -19.47 dB, and -31.47 dB, -33.49 dB respectively. The discrepancy is probably brought in by the reasons of fabrication, the difference of dielectric properties between simulation and measurement, the gap between phantom and antenna during simulation and measurement, and the cable connected to the antenna during measurement.

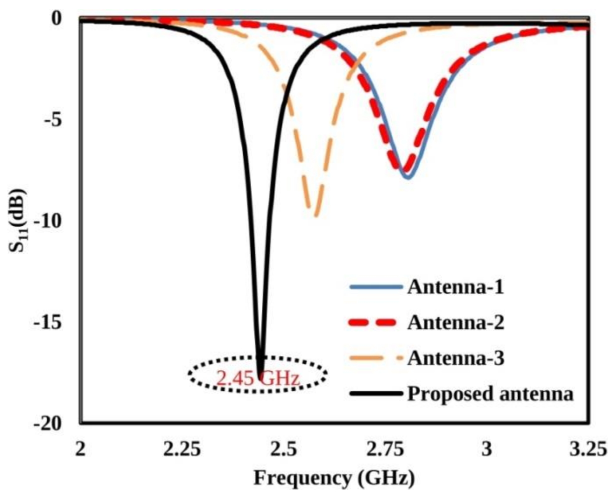

Figure 5.11 Reflection coefficient results of evaluated steps.

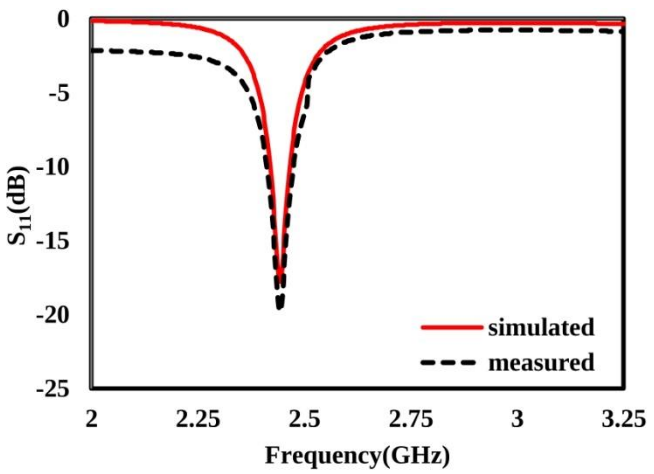

Figure 5.12 Simulated and measured reflection coefficient in free space.

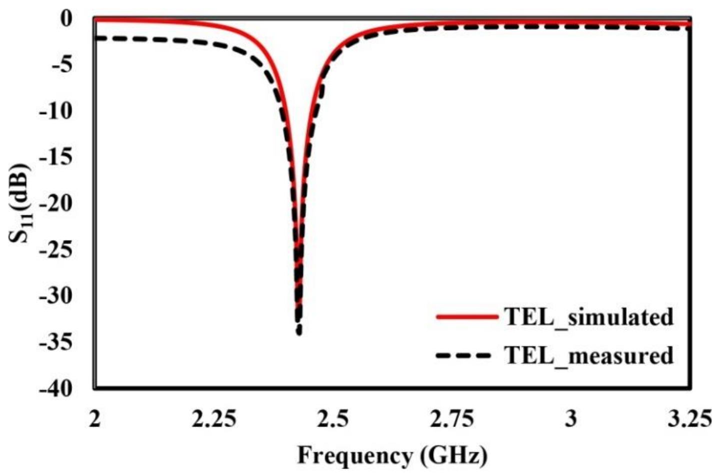

Figure 5.13 Simulated and measured reflection coefficient with TEL phantom.

5.2.5.2. Surface Current

The current density is the highest at the slot edges and decreases towards the centre of the slot. The current concentration is high at the lower end of the patch and this leads to the resonant frequency. The distribution of the current density can be affected by the dimension of the slot, the shape of the slot, the substrate material, and feeding techniques. Current density distribution is influenced by the geometry of the proposed antenna and the frequency of operation. Fig.5.14 surface current plot can provide insight into the current path and resonant behaviour of the proposed T-slot antenna. The intensity on the surface begins to decrease as the current elements go farther, with the orientation now being towards the Y-direction. The patch's centre and edges towards the X-directions have the highest intensity.

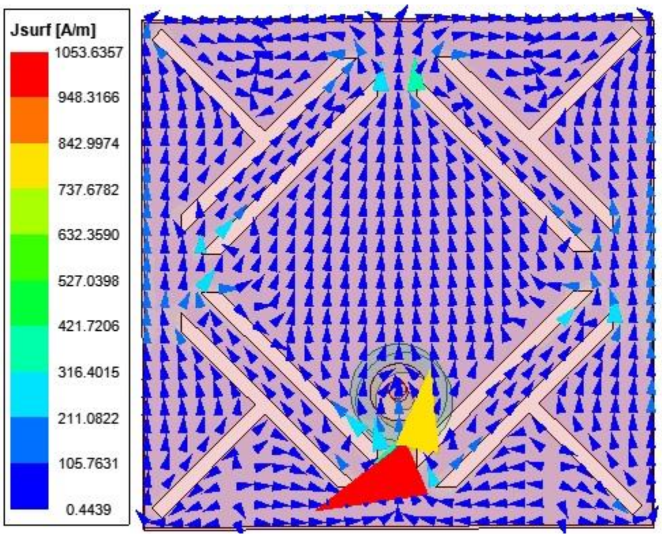

Figure 5.14 Surface current plot.

5.2.5.3. Specific Absorption Rate (SAR)

The specific absorption rate (SAR) of a slot antenna for hyperthermia application is a measure of the amount of electromagnetic energy that is absorbed by biological tissues when exposed to the antenna's electromagnetic field [99] [141]. The SAR is a crucial parameter in hyperthermia applications, as it helps to determine the amount of energy that can be safely delivered to the tissues without causing damage.

SAR values must comply with IEEE C95.1-1999 (US standard), and limit the peak average SAR value for 1g of tissue to 1.6 W/kg and 10g of tissue to 2 W/kg, respectively [29]. We perform SAR numerical analysis at 2.45 GHz with TEL phantom in HFSS software. Fig.5.15 depicts the SAR distribution at TEL, maximum SAR of 230.75 W/kg with a maximum acceptable input power of 6.93 mW in the TEL phantom, when 1W power is delivered by the proposed antenna. The dissipated power is determined by subtracting the radiated power, which is 889.92 mW, from the delivered power. The analysis SAR value of the proposed T-slot antenna encounters the IEEE evaluation standard. Also calculate the SAR value from equation (5.7), sigma (σ) conductivity and rho (ρ) mass density is taken from dielectric properties, and (E) Electric-field intensity is measured from Fig. 5.17(c).

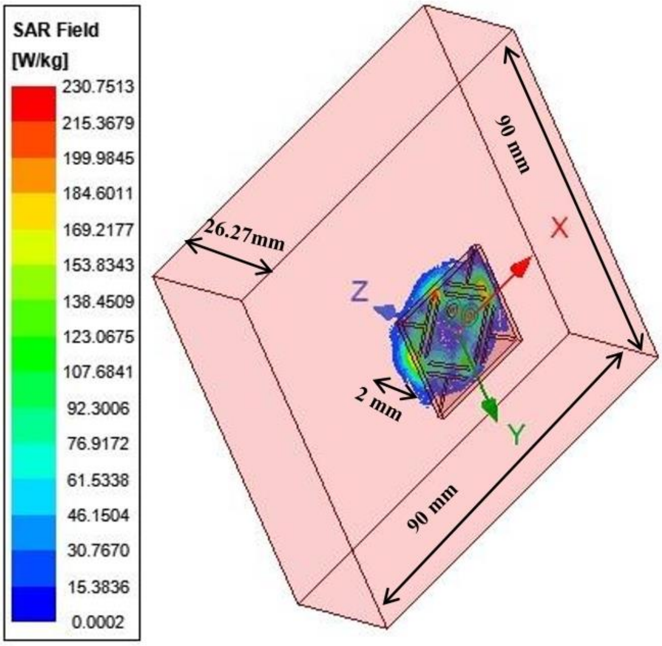

Figure 5.15 SAR plot.

5.2.5.4. Radiation Pattern

The radiation plot of the proposed T-slot antenna can be compared to that of a dipole antenna to analyze the achieved radiation patterns. While both antennas are radiating elements that operate on the principle of electromagnetic radiation, slightly different in radiation patterns due to differences in their geometry and design. A dipole antenna typically consists of two conductive elements that are equal in length and positioned parallel to each other, with a feed point at the centre. When excited by a signal, the dipole antenna radiates energy in a pattern that is typically omnidirectional in the horizontal plane but has nulls in the vertical plane. On the other hand, the proposed T-slot antenna is a planar structure that consists of a patch of conductive material on one side of a dielectric substrate, with a ground plane on the other side. For the TM_{01} mode, the contributions to the far fields are from the magnetic surface current densities on the side walls containing the radiating edges. For the TM_{01} mode, the E-plane is the X-Z plane ($\varphi=0^{\circ}$) is figure of eight having null, and the H-plane is the Y-Z plane ($\varphi=90^{\circ}$) spherical symmetry radiation pattern [142]. When excited by a signal, the proposed antenna radiates energy in a pattern that is typically directional, with a main lobe in the broadside direction and nulls in other directions.

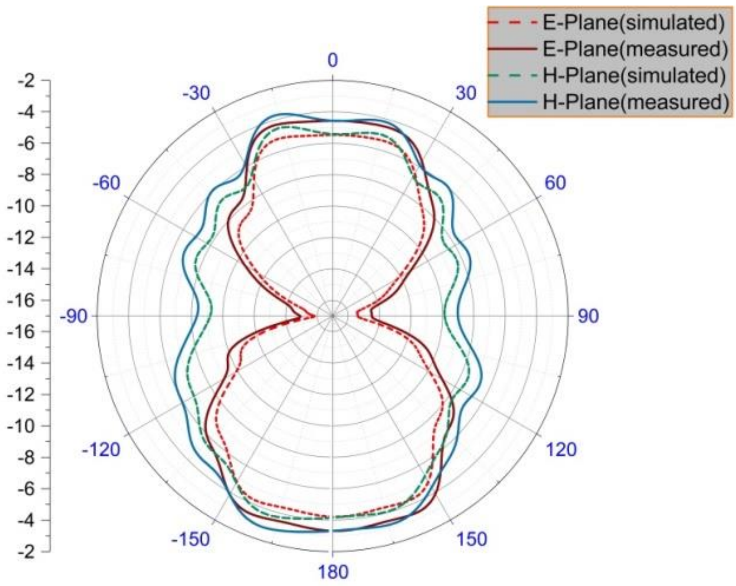

Figure 5.16 Radiation pattern plot.

Overall, the radiation pattern of this proposed antenna is typically more directional than that of a dipole antenna and meets hyperthermia application requirements. Fig.5.16 shows the simulated and measured radiation pattern plot of the E and H planes with a maximum achieved gain of -5.1 dBi.

5.2.5.5. Fabrication and Measurement

Fig.5.17(a) shows the prototype of the proposed antenna fabricated on an FR-4 substrate with a relative permittivity of 4.4 and a 1.6 mm thickness. The measurement setup for the reflection coefficient is shown in Fig.5.17(b), it was measured using an

R&S(ZNB8) vector network analyzer having a frequency range of (9kHz-8.5GHz). For the calculation of SAR first of all, measured the electric field intensity inside the TEL phantom as shown in Fig.5.17(c), in this setup, a signal generator R&S SMR 40(100 MHz-40 GHz) was used as a source, and a spectrum analyzer R&S FSH8(100 kHz-8 GHz) was used for reading the electric field intensity value. Finally, the measured SAR value was calculated using equation (5.7).

Table 5.4 Performance comparisons between previous works and this work

Ref.	Freq. (GHz)	Volume (mm^3)	S_{11} (dB)	Gain (dBi)	SAR (W/kg)	% B.W.	App.
[138]	2.45	π×5^2×1.27	-33.8	-22.7	508	8	ISM
[129]	2.4	22.5×22.5×2.5	-26	-15	N.R.	4.2	ISM
[130]	2.45	19×19.4×1.27	-24.7	-22.0	314.0	4.4	ISM
[140]	2.45	π×5.2^2×1.27	-23	-22.7	733.5	8.3	ISM
[131]	2.45	50×50×4	-21.3	4.5	N.R.	6.1	OB
[99]	2.45	32×32×3.27	-32	1.17	13.4	N.R.	ISM
[141]	2.45	22.5×22.5×2.5	-47	N.R.	3.14	N.R.	ISM
[143]	2.45	60×65×3.15	-31.2	0.5	1.75	7	OB
[144]	2.45	27×33×8	-37.5	2.19	N.R.	11.5	OB
[145]	2.45	25.9×25.9×2.5	-17.3	-23.9	0.079	14.2	ISM
[124]	2.45	π×10^2×2.54	-27	-12.3	149.7	17.6	ISM
[146]	2.4	16.5×16.5×2.54	-19	-15	292	5.7	ISM
This work	**2.45**	**26×26×1.6**	**-17.46**	**-5.1**	**230.75**	**2.85**	**ISM**

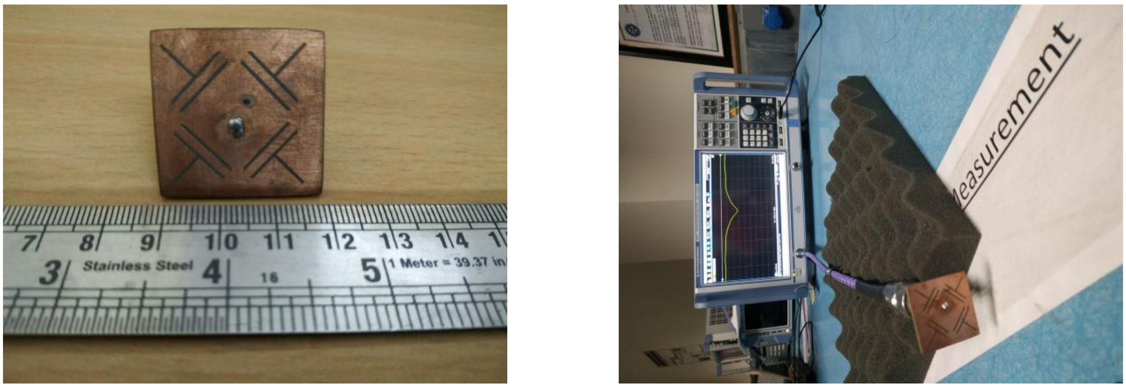

(a) Fabricated antenna (b) $|S_{11}|$ measurement

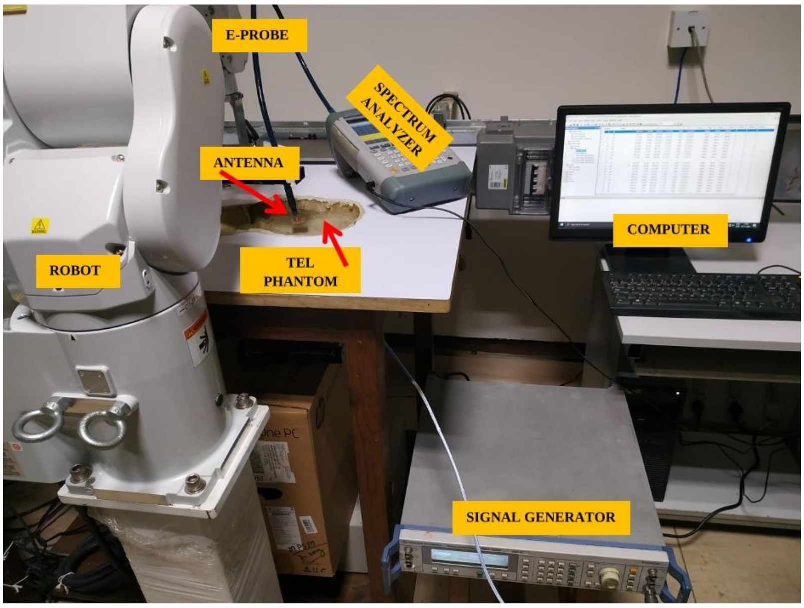

(c)Measurement setup for E-field

Figure 5.17 Fabricated prototype and measurement setup.

Finally, the results of the proposed antenna are compared to previous reports exhibited in Table 5.4. The proposed antenna has the smallest size except for reference [130] and almost higher gain compared to the reported papers.

5.2.6. Summary

The proposed corner-slot antenna has been widely used in hyperthermia applications due to its ability to efficiently generate and focus electromagnetic energy in the desired frequency range. It offers several advantages such as a low profile, easy integration with other components, and the ability to control the radiation pattern. The obtained results of the proposed antenna at 2.45 GHz are, $|S_{11}|$ is -17.46 dB, the gain of the antenna is -5.1 dBi, and SAR is 230.75 W/kg. Overall, slot antenna has shown promising results in hyperthermia applications, and ongoing research continues to improve its design and effectiveness. However, simulated and measured the SAR for careful consideration to ensure the safety and effectiveness of the treatment.

5.2.7. Conclusion

The proposed cross-slot and corner slot were designed in this chapter is most appropriate for evaluation of hyperthermia applications. Both antennas were designed and measured in TEL phantom. SAR values for both antennas are acceptable within limit of IEEE standards.

In the upcoming chapter 6, the major contributions made in the thesis, the conclusion drawn during the whole investigation, and the future scope are summarized.